Seismic Response Characteristics of Fluid-Structure Interaction in LMFBR Piping Systems

Fumio Hara
Science University of Tokyo, Tokyo, Japan

Abstract

This paper deals with a study on the vibrational response characteristics of an LMFBR piping system containing liquid sodium under one-dimensional seismic excitation. Using Z-shaped piping, we describe briefly coupled equations for the pipe's bending vibration and pressure wave, and use the basic two-degree-of-freedom vibration equations for the first modes of the piping vibration and pressure wave to obtain seismic response characteristics of the piping system. A numerical study shows that (1) the coupling effect appears between piping acceleration and liquid pressure for a piping configuration having a natural frequency ratio ν = about 0.5 to 2.0, (2) the magnitude of seismically induced pressure reaches 0.7 kPa to 1 kPa per Gal, and (3) the dead-mass model of liquid gives a nonconservative response compared to that from the pressure-wave-piping-interaction model, for which the pipe's geometrical configuration is specified.

1. Introduction

The pressure wave induced by earthquake excitation to the liquid contained in a piping system has been pointed out by Okamoto (1) and Ogawa (2), and its importance in seismic analysis of nuclear power plant (NPP) piping has been recognized for LMFBR piping systems (3) because of the following reasons: An LMFBR piping system is generally long, large in diameter, and thin-walled due to the high temperature and low pressure in operation. The mass of liquid per unit length in FBR piping thus becomes large and comparable with that of the pipe itself. These characteristics of the piping system may reduce the natural frequency of the pressure wave and induce vibrational coupling in the piping's response to seismic excitation. The magnitude of the induced pressure wave may thus become comparable to that of normal operation pressure. It is thus necessary in the seismic analysis of FBR piping system to take into account the pressure wave of the liquid contained in a pipe caused by earthquake excitation.

This paper is a basic study on the vibrational response characteristics of an LMFBR piping system containing liquid sodium undergoing one-dimensional seismic excitation. Using Z-shaped piping, we describe coupled equations for the pipe's bending vibration and pressure wave (3). Applying modal expansion to the governing equations, we obtain the two-degree-of-freedom vibration equations for the first vibration modes of the pipe bending and pressure wave. We first investigate the characteristics of the mass ratio between the pipe and liquid, and the natural frequency ratio between the pipe' bending and pressure wave vibrations with respect to pipe configuration. Changing the ratio of natural frequencies between the pipe vibration and pressure wave, we calculate seismic responses for the pipe acceleration and pressure in liquid, and obtain the effects of the seismically induced pressure wave on piping vibration. Results are compared with those obtained from a "dead-mass model" of liquid. Numerical results show: (1) the coupling appears between piping vibration and pressure wave

for a conventional FBR piping system. (2) The magnitude of seismically induced pressure wave may reach 0.7 kPa to 1 kPa per Gal, equivalent to 7 to 10 Atm for 1 G of seismic excitation. (3) The dead-mass model of liquid gives a nonconservative response to the FBR piping system compared to that from the model taking into account coupling between the pipe vibration and pressure wave, for which the pipe's geometrical configuration is specified by the vibration parameters.

2. Brief Description of the Equation of Motion

Two-dimensional Z-shaped piping is used in the following theoretical formulation for a coupled vibrational response caused by one-dimensional seismic excitation, where the assumptions are that

(1) liquid contained in the pipe is compressible,
(2) friction loss on the pipe's inner surface is negligible,
(3) the pipe's bending vibration and pressure wave are small,
(4) the pipe's radial and axial deformations are neglected, and
(5) the gravity force is neglected to simplify the formulation and to extract basic vibrational features of a pressure-wave-piping-interaction system.

2.1 Coupled vibration equation

Fig. 1 is a schematic drawing of two-dimensional Z-shaped piping whose both ends, A and B, are anchored. At points C and E, the piping is simply supported and section II slides in the y direction due to a sliding support installed at point D. The parts indicated by A-C and E-B in both sections I and III are assumed not to vibrate. The piping system in Fig. 1 thus vibrates only in part C-D-E, where section II is assumed to move in the y direction like a rigid body, and parts C-F and G-E vibrate laterally.

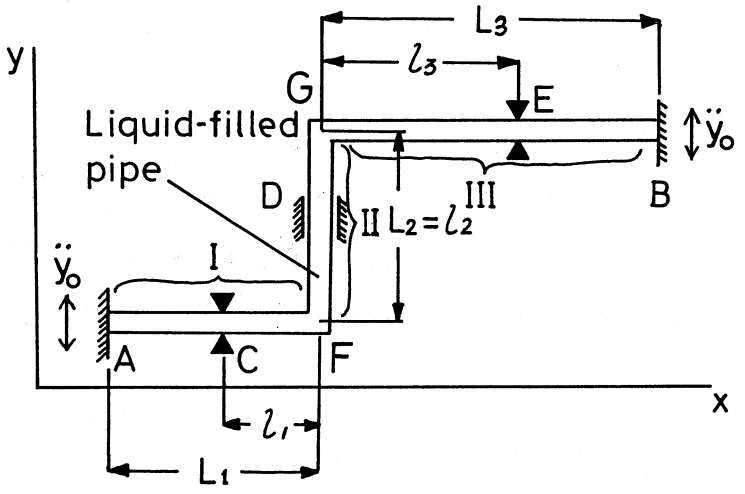

Fig. 1 Z-shaped piping used in the analysis

Let the coordinate x be in the pipe's axis at equilibrium and y normal to it, and seismic displacement y_0 be identical at points A, B, C, and E. Note that the origin of the x axis is point A for liquid wave or C for the pipe vibration and that the notation of x is not differentiated in the formulation below σ. Considering force balance in the x and y directions at a small pipe element δ x

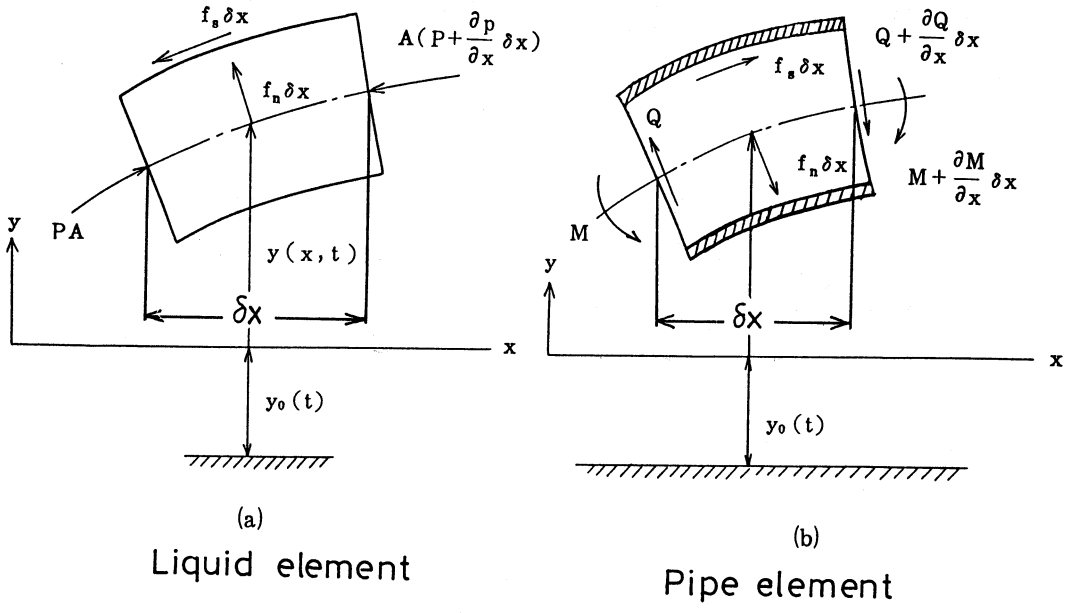

Fig. 2 Liquid and pipe elements for force balance in the x and y directions

containing liquid, the liquid and structure elements are taken out as shown in Figs. 2 (a) and (b), where the normal and tangential forces to the deformed pipe axis are defined as f_n and f_s per unit length. Designating the pipe's hydraulic cross section by A, bending moment by M, pressure by p, shear force by Q, the induced liquid velocity by u, pipe's vibrational displacement by y, and the liquid density by ρ, the following four equations hold in the x and y directions for the liquid and structure elements:

For the liquid element

$$-A\frac{\partial p}{\partial x}-f_s-f_n\frac{\partial y}{\partial x}-\rho A\left(\frac{\partial u}{\partial t}+u\frac{\partial u}{\partial x}\right)=0 \qquad (1)$$

$$f_n-A\frac{\partial}{\partial x}\left(P\frac{\partial y}{\partial x}\right)-f_s\frac{\partial y}{\partial x}$$

$$-\rho A\left\{\left(\frac{\partial}{\partial t}+u\frac{\partial}{\partial x}\right)^2 y+\frac{d^2y_0}{dt^2}\right\}=0 \qquad (2)$$

and for the pipe element

$$f_s+f_n\frac{\partial y}{\partial x}+\frac{\partial}{\partial x}\left(Q\frac{\partial y}{\partial x}\right)=0 \qquad (3)$$

$$-\frac{\partial Q}{\partial x}-f_n+f_s\frac{\partial y}{\partial x}-C\frac{\partial y}{\partial t}-m\frac{\partial^2 y}{\partial t^2}-m\frac{d^2y_0}{dt_2}=0 \qquad (4)$$

We use the following relationship between the moment M and the shear force Q

$$Q=-\frac{\partial M}{\partial x}=+EI\frac{\partial^3 y}{\partial x_3} \qquad (5)$$

and the continuity equation for liquid motion

$$\frac{\partial p}{\partial t}=-K\frac{\partial u}{\partial x} \qquad (6)$$

where K is the volumetric stiffness of liquid.

Substituting the term $f_s + f_n \partial y/\partial x$, obtained from eq. (3), into eq. (1), using the relationship in eq. (5), and further neglecting higher order terms, a conventional equation for the force balance in the liquid element is

$$-A\frac{\partial p}{\partial x}=\rho A\frac{\partial u}{\partial t} \tag{7}$$

From eqs. (6) and (7), we obtain a linear pressure wave equation

$$\frac{\partial^2 p}{\partial t^2}=C^2\frac{\partial^2 p}{\partial x^2},\quad C^2=K/\rho \tag{8}$$

Substituting the term $f_n - f_s \partial y/\partial x$ obtained from eq. (2) into eq. (4), and using eq. (5), and neglecting the higher order terms, the pipe's vibration equation becomes simple, as shown in eq. (9).

$$EI\frac{\partial^4 y}{\partial x^4}+C\frac{\partial y}{\partial t}+(m+\rho A)\frac{\partial^2 y}{\partial t^2}=-(m+\rho A)\frac{d^2 y_0}{dt^2} \tag{9}$$

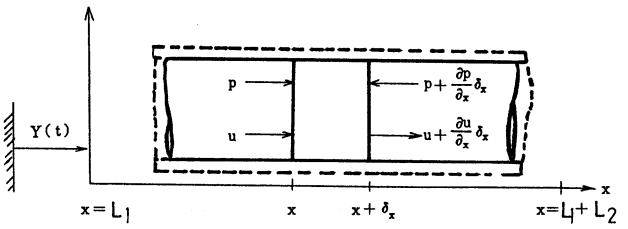

Fig. 3 Pressure and velocity induced in pipe part II

Fig. 3 is an illustration of seismically induced pressure and liquid velocity acting on a small liquid element in part II, where the absolute coordinates of the element are

$$X=x+Y,\ Y+y(l_1,t)+y_0(t) \tag{10}$$

Considering the force balance at the liquid element, we obtain

$$-\frac{\partial p}{\partial x}=\rho\frac{\partial u}{\partial t}+\rho\frac{d^2 Y}{dt^2}h(x) \tag{11}$$

where the function h(x) is defined as h(x) = 1 for $L_1 \leq x \leq L_1 + L_2$, and h(x) = 0 otherwise. From eqs.(6) and (11), the following pressure wave equation is obtained

$$\frac{\partial^2 p}{\partial t^2}=C^2\frac{\partial^2 p}{\partial x^2}+K\frac{d^2 Y}{dt^2}[\delta(x-l_1)-\delta\{x-(l_1+l_2)\}] \tag{12}$$

where the second term in the right side of eq. (12) is an excitation due to the pipe's vibration.

The boundary conditions for the piping are defined as follows: For pipe part I, point A is simply supported and thus, at x = 0, y and y'' are zero. At elbow F, or $x = l_1$, a load $(p(L_1)A - ml_2 \ddot{Y})\ \delta(x - l_1)$ is applied. Point E of pipe part III is also simply supported and thus, at $x = l = l_1 + l_3$, y and y'' are zero. At

the other elbow, G, a load due to pressure and mass of part II ($p(L_1 + L_2)A + ml_2\ddot{Y}$) $\delta(x - l_1 - l_3)$ is applied. At interboundary $x = l_1$, the pipe's vibrational displacements, $y(l_1)$ for the part I and $y(l_1)$ for part III, should be identical.

For liquid wave motion, both ends A and B of the piping are closed, or $\partial p/\partial x = 0$ for $x = 0$ and $x = L = L_1 + L_2 + L_3$. At elbows F and G, the pressure and velocity must be continuous.

2.2 Modal vibration equation

Bending vibration in the piping is governed by eq. (9) for parts I and III, and pipe part II is assumed as a rigid body. Thus, we can contract part II to a volumeless point with a mass of ml_2, ($l_2 = L_2$) as shown in Fig. 4. Inertia force $ml_2\ddot{Y}$ and the pressure force caused by the pressure difference between points F and G act on the vibrating piping at point $x = l_1$ for the model of the piping system. We thus derive the vibration equation as

$$EI\frac{\partial^4 y}{\partial x^4} + C\frac{\partial y}{\partial t} + (m+\rho A)\frac{\partial^2 y}{\partial t^2} = -(m+\rho A)\frac{d^2 y_0}{dt^2} + [\{P(L_1+L_2) - P(L_1)\}A - ml_2\ddot{Y}]\delta(x-l_1) \qquad (13)$$

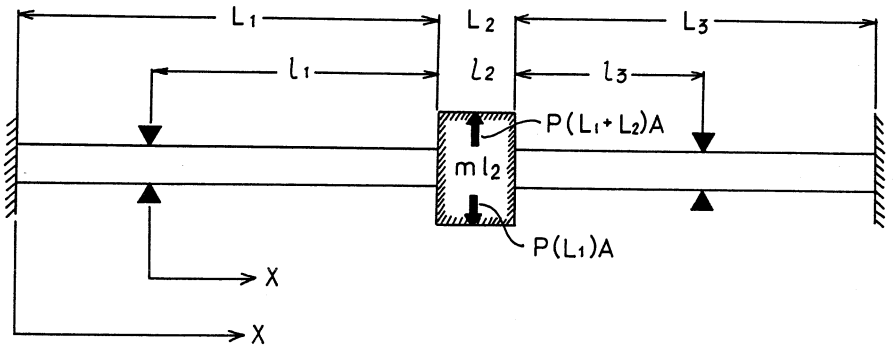

Fig. 4 Lumped-parameter model of pipe part II in Z-shaped piping

Assuming eigen-functions for pressure wave and bending vibration as $\cos(\pi x/L)$ and $\sin(\pi x/l)$, the pipe's displacement, y, and pressure, p, are expressed as

$$y = f_1(t)\sin\pi x/l,\ l = l_1 + l_3$$
$$p = f_2(t)\cos\pi x/L,\ L = L_1 + L_2 + L_3 \qquad (14)$$

Substituting these expressions into eq. (13) and applying modal expansion to the equation, we obtain the following

$$\ddot{f}_1 + 2w_n\zeta f_1 + w_n^2 f_1 - a f_2 = -b\ddot{y}_0 \qquad (15)$$

where

$$\alpha_1 = l_1/l,\ \alpha_2 = l_2/l,\ \beta_1 = L_1/L,\ \beta_2 = L_2/L$$
$$M = (m+\rho A) + 2m\alpha_2\sin^2\alpha_1\pi$$
$$w_n = \sqrt{EI\left(\frac{\pi}{l}\right)^4/M}$$

$$\zeta = C/2w_n$$
$$a = 2A\sin\alpha_1\pi(\cos(\beta_1+\beta_2)\pi - \cos\beta_1\pi)/Ml$$
$$b = \{4(m+\rho A)/\pi + 2m\alpha_2\sin\alpha_1\pi\}/M$$

The pressure wave is governed by eqs. (8) and (12) for pipe parts I and III, and II. Taking into account the mathematical property of the δ-function, eq. (12) holds for the entire interval of $0 \leqq x \leqq L$. Using the expression for p and y shown in eq. (14) and employing the same technique as before, we obtain the equation

$$\ddot{f}_2 + w_p^2 f_2 - d\,\ddot{f}_1 = e\,\ddot{y}_0 \qquad (16)$$

where

$$w_p = \left(\frac{\pi c}{L}\right)$$
$$d = 2K\sin\alpha_1\pi(\cos\beta_1\pi - \cos(\beta_1+\beta_2)\pi)/L$$
$$e = 2K(\cos\beta_1\pi - \cos(\beta_1+\beta_2)\pi)/L$$

Combining eqs. (15) and (16), the coupled vibration between the pressure wave and pipe bending is expressed as

$$\begin{bmatrix} 1 & 0 \\ -d & 1 \end{bmatrix}\begin{bmatrix} \ddot{f}_1 \\ \ddot{f}_2 \end{bmatrix} + \begin{bmatrix} 2w_n\zeta & 0 \\ 0 & 0 \end{bmatrix}\begin{bmatrix} \dot{f}_1 \\ \dot{f}_2 \end{bmatrix}$$
$$+ \begin{bmatrix} w_n^2 & -a \\ 0 & w_p^2 \end{bmatrix}\begin{bmatrix} f_1 \\ f_2 \end{bmatrix} = \begin{bmatrix} -b \\ e \end{bmatrix}\ddot{y}_0 \qquad (17)$$

Introducing two parameters, s_1 and s_2, to normalize these values; f_1, y_0, and f_2 are then

$$f_1 = s_1\phi_1,\ y_0 = s_1,\ \eta_0,\ f_2 = s_2\phi_2 \qquad (18)$$

and also $\tau = w_n t$ and $\nu = w_p/w_n$, the following equation is obtained for the coupled modal vibration

$$\ddot{\phi}_1 + 2\zeta\dot{\phi}_1 + \phi_1 - \alpha\phi_2 = -\beta\ddot{\eta}_0$$
$$\ddot{\phi}_2 + \nu^2\phi_2 - \gamma\ddot{\phi}_1 = \epsilon\ddot{\eta}_0 \qquad (19)$$

where α, β, γ, and ε are

$$\alpha = s_2 a/s_1 w_n^2,\ \beta = b,\quad \gamma = ds_1/s_2,\ \epsilon = es_1/s_2$$

3. Mass Ratio and Frequency Ratio

In eq. (17), the coupling effects are expressed by two parameters, a and d, which are related to the mass of pipe including liquid per unit length and to the volumeric stiffness of the liquid. As the parameter a is determined by the geometrical configuration parameters such as pipe diameter, thickness, and length as well as material parameter such as density; and the parameter d represents the characteristic of the liquid pressure wave, we employ the follwing two parameters

μ = mass ratio = $\rho A/M$, $\nu = w_p/w_n$ (20)

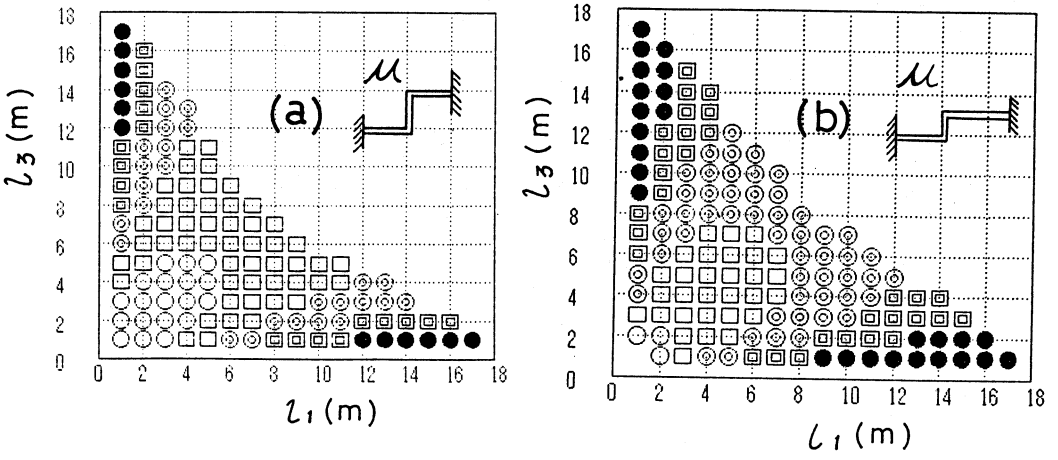

Fig. 5 Mass ratio μ distribution with respect to the piping support location l_1 and l_3, (a) L_1 = L_2 = L_3 = 20 m, (b) L_1=20m, L_2 = 10 m, and L_3 = 30 m
○~0.2; □ 0.2~0.4; ◎ 0.4~0.6; ▣ 0.6~0.8; ● 0.8~1.0

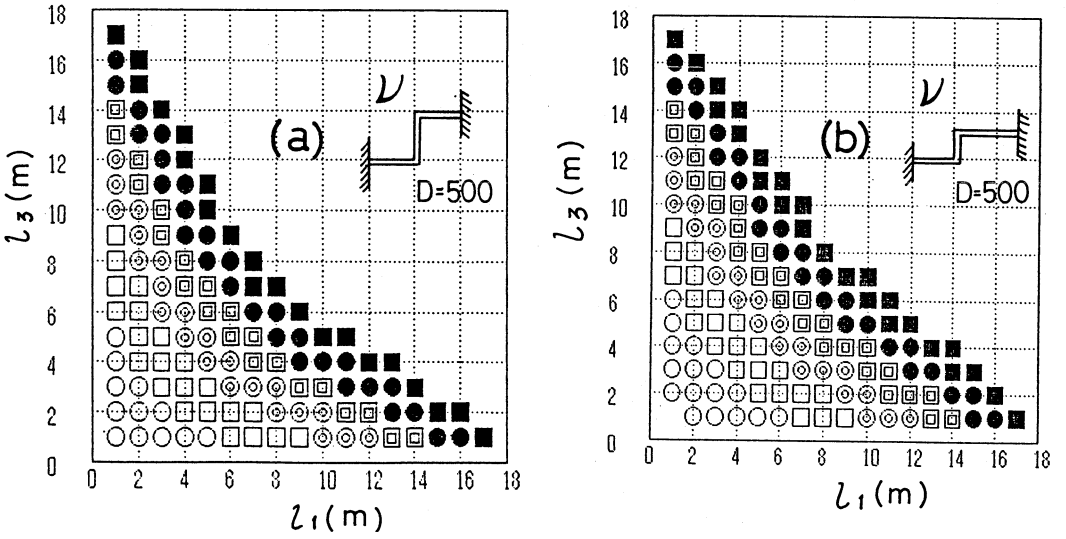

Fig. 6 Frequency ratio ν distribution with respect to the piping support location l_1 and l_3, (a) L_1 = l_2 = L_3 = 20 m, (b) L_1 = 20 m, L_2 = 10 m, and L_3 = 30 m
○~0.5; □0.5~1.0; ◎ 1.0~1.4; ▣ 1.5~2.0; ● 2.0~2.5; ■ 2.5~3.0

to investigate the basic relationship of these parameters to the configuration of the piping concerned.

We calculated the values of μ and ν for each l_1 and l_3 in the three different configurations of the pipe with 0.508 m in diameter and 0.0152 m thick, i.e., (A) L_1 = L_2 = L_3 = 20 m; (B) L_1 = 20 m, L_2 = 10 m and L_3 = 30 m. The

results are shown in Fig. 5 for the mass ratio μ, and in Fig. 6 for the frequency ratio ν. Fig. 5 (a) is for the piping configuration (A) $L_1 = L_2 = L_3 = 20$ m and (B) for $L_1 = 20$m, $L_2 = 10$ m, and $L_3 = 30$ m. For both the configurations, the large value of mass ratio appears for asymmetrical support locations; i.e., l_1 = large and l_3 = small or vis-versa. The symmetrical support locations with respect to the center part of pipe; i.e., the part II in Fig. 1, the mass ratio becomes small. Fig. 5 (b) shows the similar feature of the mass ratio distribution with respect to the support location parameters l_1 and l_2, even for the asymmetric piping configuration (B) $L_1 = 20$ m, $L_2 = 10$ m, and $L_3 = 30$ m.

In Fig. 6 (a) the large frequency ratio appears in the support location such that $l_1 + l_3$ = a large value like 18, and the small frequency ratio in the support location such as $l_1 + l_2$ = a small value, e.g., 2 to 4. The same feature is seen even for the asymmetric piping configuration as shown in Fig. 6 (b).

4. Numerical Analysis

Numerically solving the vibration equation of a single-degree-of-freedom system

$$\ddot{\xi}_o + 2\zeta_e w_e \dot{\xi}_0 + w_e^2 \xi_o = R \qquad (21)$$

where R on the right side of the equation is a time series of random numbers uniformly distributed, cutting off the very initial part of the response, ξ_o, to obtain a stationary random acceleration, and multiplying the envelope function, defined as $E(\tau) = \exp(-0.00417\tau) - \exp(-0.00833\tau)$, with it, we obtain a nonstationary seismic acceleration, η_o, to be applied to eq. (19). Setting the initial conditions for pressure and pipe bending vibration as $\phi_1 = \dot{\phi}_1 = 0$, and $\phi_2 = \dot{\phi}_2 = 0$, we solve the governing eq. (19) using the Runge-Kutta-Gill method with a time step of 0.2 in terms of a normalized τ.

We calculate the responses of pressure and the pipe's vibrational acceleration, and evaluate the response multiplication factor defined as the ratio of their root mean square values to that of the input acceleration.

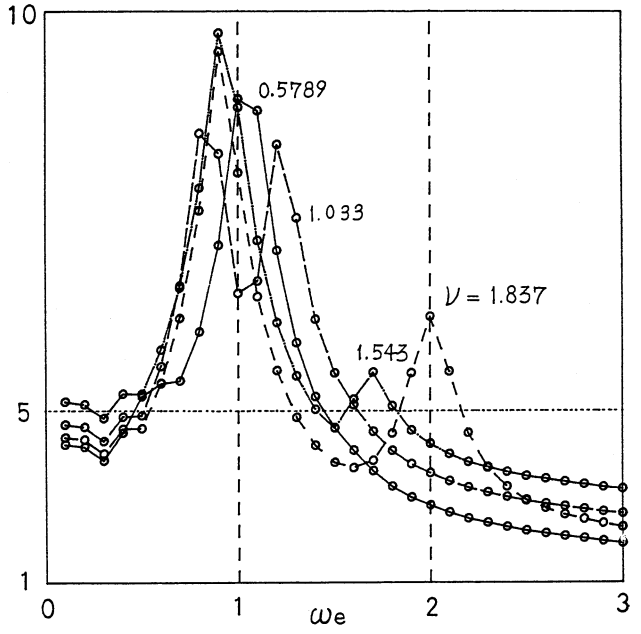

Fig. 7 Seismic acceleration response spectrum for piping with $L_1 = 20$ m, $L_2 = 10$ m, and $L_3 = 30$ m

Changing the dominant frequency of the seismic input ω_e from 0 to 3, we obtain a frequency spectrum of the response multiplication factor. To clarify the vibrational characteristics of the pressure-wave-piping-interaction system, we calculate the frequency spectrum for various cases of the natural frequency ratio ν between the pressure wave and pipe vibration.

We also calculate the frequency spectrum of response multiplication factor using the dead-mass model of liquid contained in the piping and compare the maximum values for both models to clarify the effects of the pressure wave.

4.1 Frequency spectrum

Fig. 7 is the frequency spectrum of acceleration response multiplication factor for the piping 60 m long, 0.2163 m in diameter, and 0.0082 m thick; L_1, L_2, and L_3 are 20, 10, and 30 m. When the frequency ratio between the pressure wave and pipe vibration is small, for example $\nu = w_p/w_n = 0.5789$, the spectrum is nearly single-peaked at the piping's natural frequency. The frequency ratio becomes nearly one, the response factor spectrum is doubly peaked, and the magnitude of the peaks is rather smaller than that of other frequency ratios. When the piping's natural frequency is far smaller than that of the pressure wave, for instance, ν = 1.543 or 1.837, a single peak dominates at ω_e = 1 and its magnitude is about 30% higher than that for ν = 1.

Fig. 8 is the frequency spectrum for the pressure wave, which is always doubly peaked. The maximum peak value reachs about 100 kPa per 100 Gal. When the frequency ratio ν is small, e.g., ν = 0.5789, the maximum peak appears at its natural frequency but, as it enlarges, both peaks induced by the pipe vibration and seismic excitation to the pressure wave become comparable.

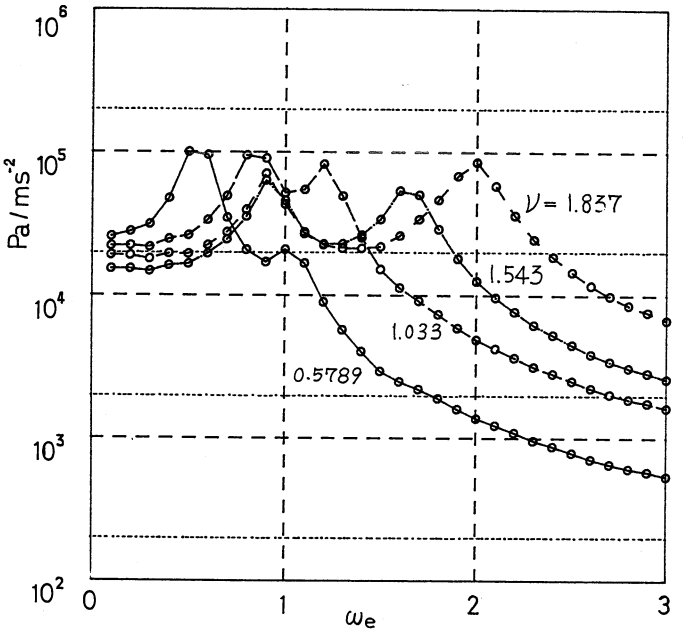

Fig. 8 Seismic pressure response spectrum for the same piping as in Fig. 7

4.2 Maximum response factor

The maximum value of the frequency spectrum of the response multiplication factor of acceleration, defined as H max = (the peak value of frequency spectrum for the pipe-acceleation response multiplication factors) is evaluated for the

two piping configurations, i. e., (A) $L_1 = L_2 = L_3 = 20$ m and (B) $L_1 = 20$ m, $L_2 = 10$ m, $L_3 = 30$ m with changing the support location l_1 and l_3. The results are shown in Figs. 9 (a) and (b), where (a) is for the piping configuration (A) $L_1 = L_2 = L_3 = 20$ m, and (b) for (B) $L_1 = 20$ m, $L_2 = 10$ m, and $L_3 = 30$ m. The high acceleration response appears in the symmetric piping configuration with asymmetric support location as seen in Fig. 10 (a), but in asymmetric piping configuration like (B) in Fig. 10 (b), the high response appears at asymmetric support location, say, $l_1 + l_2 = 10$.

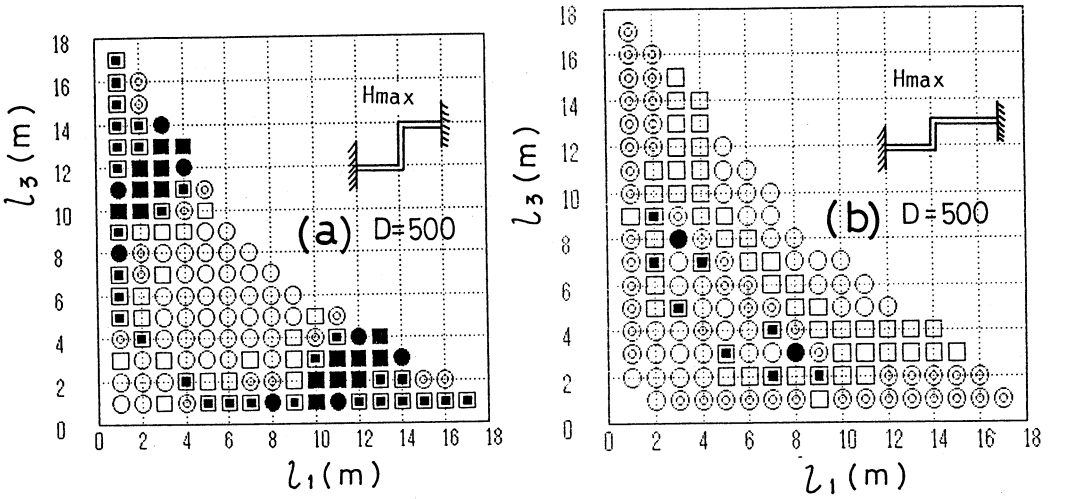

Fig. 9 Maximum of the response multiplication frequency spectrum H max for the pipe-acceleration response with respect to the support location l_1 and l_3, (a) $L_1 = L_2 = L_3 = 20$ m, (b) $L_1 = 20$ m, $L_2 = 10$ m, and $L_3 = 30$ m
○~8; □ 8~9; ◎ 9~10; ▣ 10~11; ● 11~12; ■ 12~

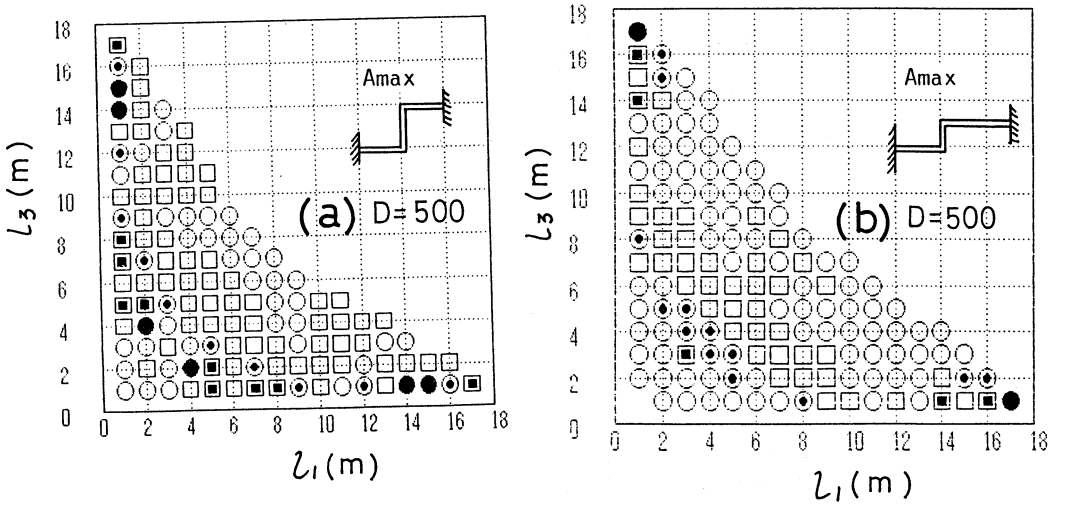

Fig. 10 Maximum of the response multiplication frequency spectrum Amax for the pressure wave response with respect to the support location l_1 and l_3, (a) $L_1 = L_2 = l_3 = 20$ m, (b) $L_1 = 20$ m, $l_2 = 10$ m, and $l_3 = 30$ m
○~1; □ 1~2; ◉ 2~3; ▣ 3~4; ● 4~5; ■ 5~ (100 kPa)

The maximum value of the frequency spectrum for the pressure multiplication factor, defined A max = (the peak value of frequency spectrum for pressure-response multiplication factors) is also evaluated and the results are shown in Figs. 10 (a) and (b) for the two piping configurations (A) and (B). For both symmetric and asymetric piping configurations, (A) and (B), the high pressure response appears in the peculiar support location such as $l_1 \times l_3 = 16$.

4.3 Maximum response ratio between "interaction and dead-mass models"

The maximum response ratios κ of the response spectrum of the piping acceleration are compared between the interaction and dead-mass models using two piping configurations, i.e., L_1, L_2, and L_3 are (A) all 20 m; and (B) 20, 10, and 30 m.

Fig. 11(a) is a map of the maximum response ratio κ between the dead-mass and the pressure-wave-piping-interaction models for piping (A). The vertical and horizontal axes are l_1, and l_3; i.e., the length in meters, of pipe parts C-F and G-E. Depending on the piping configuration, the piping response to seismic excitation differs for the models used in the analysis. When l_1 and/or l_2 are 2 to 5 m, the dead-mass model gives an unconservative value to the highest response factor compared to the pressure-wave-piping-interaction model. When they are 7 to 9 m, however, the dead-mass model offers a conservative value.

Fig. 11(b) is the result for piping (B), where the symbols mean the same as before. When the piping has a configuration where $l_1 + l_3 = 10$ to 14, the dead-mass model gives an unconservative value to the highest response factor, and the result from the dead-mass model is conservative for pipings where $l_1 + l_3 = 6$ to 9 m.

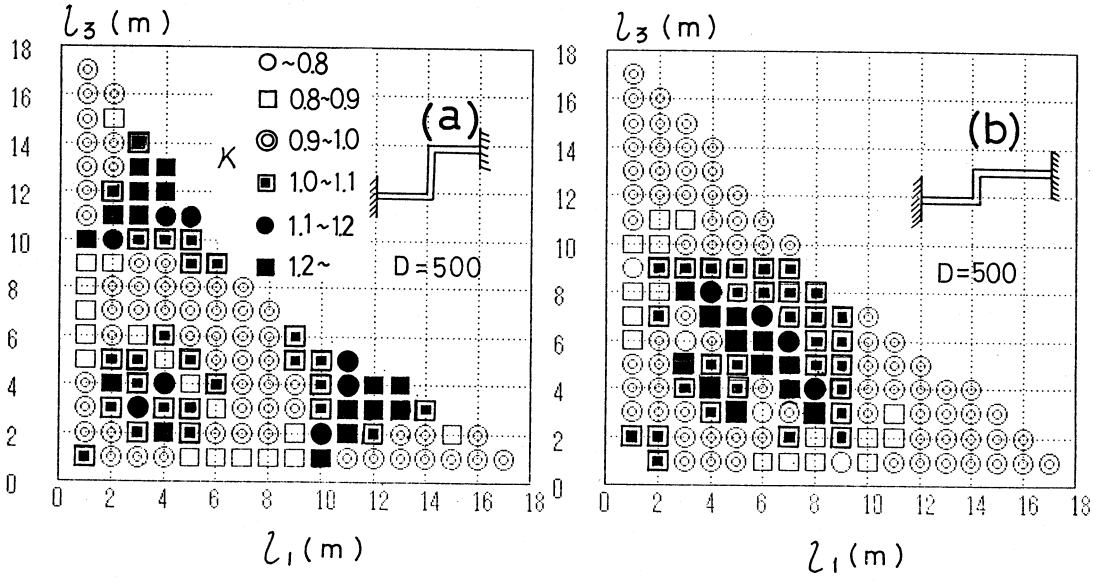

Fig. 11 Map of the vibration model giving the highest response factor κ for piping configuration (a) $L_1 = L_2 = L_3 = 20$ m; (b) $L_1 = 20$, $L_2 = 10$, $L_3 = 30$ m

4.4 Response factor ratio with regard to ratios μ and ν

For the particular two values of the dominant frequency of seismic input acceleration ω_e, we evaluated the ratio ε of acceleration multiplication factors between the interaction and dead-mass models for various mass ratio μ and frequency ratio ν in the case of the piping configuration A; i.e., $L_1 = L_2 = L_1 = 20$ m. Fig. 12(a) is the map of the ratio ε for $\omega_e = 0.5$, showing that, for a particular area hatched in the map, the dead-mass model of the liquid contained

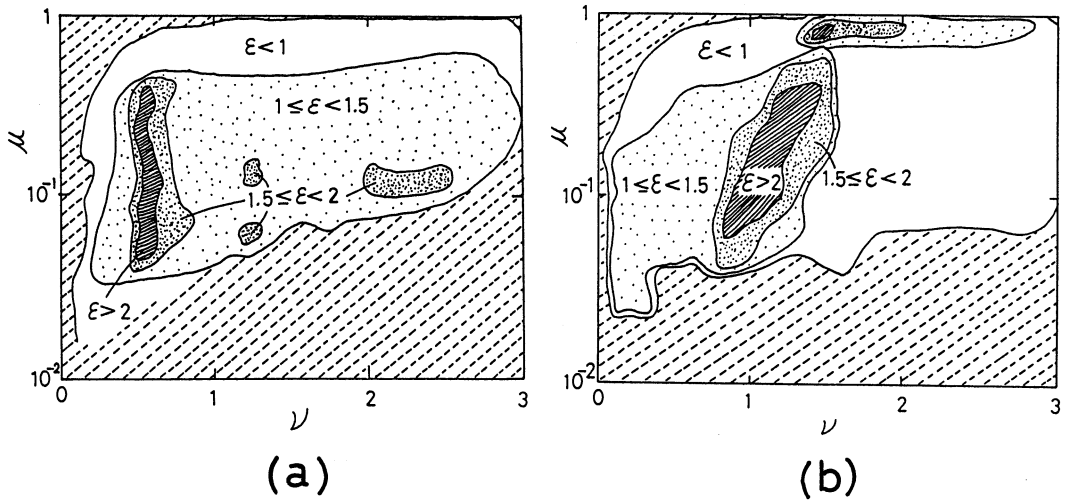

Fig. 12 Map of response factor ratio ε with respect to μ and ν between the dead-mass model and pressure-wave-structure interaction model for (a) ω_e = 0.5 and (b) ω_e = 1.5

in the pipe gives an unconservative response compared with that obtained by the interaction model between pipe's bending vibration and pressure wave. Fig. 12(b) is the result for ω_e = 1.5, showing the same feature as in Fig. 12(a) concerning the response conservatism.

5. Conclusion

This paper numerically investigated the seismic response characteristics of fluid-structrue interaction in LMFBR piping systems according to the theoretically formulated coupled vibration between a pipe's bending and pressure wave under seismic excitation. Based on the equation of two-degree-of-freedom vibration system for the first modes of both the piping vibration and pressure wave, and using nonstationary random, seismic acceleration generated artificially, we calculated response multiplication factors for a number of piping configurations, and found the followings: (1) Fluid-structure coupling effects on the vibration response of piping appeared markedly for a piping system having a natural frequency ratio ν from about 0.5 to 2.0. (2) The magnitude of the pressure wave induced by coupling reached about 0.7 to 1.0 kPa per 1 Gal. (3) The dead mass-model of the liquid contained in the pipe gave unconservative results for the response multiplication factor, which is dependent strongly on the piping configuration.

Further studies on the modeling of the interaction between the pressure wave and piping, with numerical analyses for acutual piping systems, are needed to clarify the general characteristics of the coupled vibrations between liquid and piping structures and to derive useful knowledge about the seismic design of LMFBR piping systems.

References

(1) Okamoto, S., "Introduction to Earthquake Engineering", Univ. of Tokyo Press, (1984), p. 629
(2) Ogawa, N., "Seismic Response of Liquid and Piping, 1st Report", Trans. JSME, Vol. 51, No. 468, (1985), pp. 1960 - 1966
(3) Hara, F., "Seismic Vibration Analysis of Fluid-Structure Interaction in LMFBR Piping Systems", ASME J. Pressure Vessel Tech. Vol. 110, May 1988, pp. 177-181